NeuroImage 237 (2021) 118116

Contents lists available at ScienceDirect

NeuroImage

journal homepage: www.elsevier.com/locate/neuroimage

Bloch modelling enables robust T2 mapping using retrospective proton density and T2-weighted images from different vendors and sites

Gitanjali Chhetri[a], Kelly C. McPhee[b,1], Alan H. Wilman[a,b,*], Alzheimer's Disease Neuroimaging Initiative[2]

[a] Department of Biomedical Engineering, University of Alberta, 1098 RTF, Edmonton, AB T6G 2V2, Canada
[b] Department of Physics, University of Alberta, 4-181 CCIS, Edmonton, AB T6G 2E1, Canada

ARTICLE INFO

Keywords:
T2-weighting
Proton density
Stimulated echoes
Fast spin echo
T2 quantification

ABSTRACT

T2 quantification is commonly attempted by applying an exponential fit to proton density (PD) and transverse relaxation (T2)-weighted fast spin echo (FSE) images. However, inter-site studies have noted systematic differences between vendors in T2 maps computed via standard exponential fitting due to imperfect slice refocusing, different refocusing angles and transmit field ($B1^+$) inhomogeneity. We examine T2 mapping at 3T across 13 sites and two vendors in healthy volunteers from the Alzheimer's Disease Neuroimaging Initiative (ADNI) database using both a standard exponential and a Bloch modelling approach. The standard exponential approach resulted in highly variable T2 values across different sites and vendors. The two-echo fitting method based on Bloch equation modelling of the pulse sequence with prior knowledge of the nominal refocusing angles, slice profiles, and estimated $B1^+$ maps yielded similar T2 values across sites and vendors by accounting for the effects of indirect and stimulated echoes. By modelling the actual refocusing angles used, T2 quantification from PD and T2-weighted images can be applied in studies across multiple sites and vendors.

1. Introduction

Transverse relaxation (T2) time is one of the fundamental contrast mechanisms in MRI. It is highly sensitive to a wide range of tissue pathologies including inflammation, iron accumulation, neurodegeneration and calcification (Bartzokis et al., 2004; Cheng et al., 2012; Deoni, 2010; MacKay et al., 2006; Schenck and Zimmerman, 2004; Vymazal et al., 1999). For T2 mapping, multiple echo spin echo (MESE) methods are commonly used; however fitting the decay curve with a standard exponential function often results in grossly overestimated T2 values. Inaccuracies in T2 values from fitting with an exponential decay curve arise from three main sources of error, all of which contribute to the presence of stimulated or indirect echoes because the refocusing pulses are not ideal (Hennig, 1991; Lebel and Wilman, 2010; Majumdar et al., 1986). First, nominal refocusing flip angles less than 180° may be employed to mitigate specific absorption rate problems. Second, non-rectangular slice profiles lead to a variation of flip angles across the slice. Third, substantial radiofrequency (RF) interference effects occur at field strengths 3T and higher, and to a lesser extent at lower field strengths, which causes flip angles to vary from their nominal value across the imaging volume. There is a large body of literature that uses T2 modelling methods to account for the above mentioned effects, mainly using MESE but also acquisition of fast spin echo (FSE) sequences at different echo times (TEs) (Lebel and Wilman, 2010; Prasloski et al., 2012; Ben-Eliezer et al., 2015; McPhee and Wilman, 2015; Petrovic et al., 2015; Nöth et al., 2017; Emmerich et al., 2019). In the current work, the focus is fitting of the dual-echo FSE sequence.

Dual-echo FSE or turbo spin echo (TSE) sequences (Hennig et al., 1986) are used in clinical MRI applications enabling high-resolution proton density (PD) and T2-weighted contrast. Many authors have attempted to estimate T2 by fitting a simple exponential decay function to the two PD and T2-weighted FSE images (Bauer et al., 2010; Hasan et al., 2010; Knight et al., 2016; Sedlacik et al., 2014). However, in a two-point exponential fit using PD-weighted and T2-weighted images, the limitations of stimulated echoes are similar to the MESE methods de-

* Corresponding authors.
E-mail addresses: chhetri@ualberta.ca (G. Chhetri), wilman@ualberta.ca (A.H. Wilman).
[1] Present address for Kelly C. McPhee: Department of Medical Physics, CancerCare Manitoba, 675 McDermot Avenue, Winnipeg, Manitoba R3E 0V9, Canada
[2] Data used in the preparation for this article were obtained from the Alzheimer's Disease Neuroimaging Initiative (ADNI) database (https://ida.loni.usc.edu/login.jsp?project=ADNI). As such, the investigators within the ADNI contributed to the design and implementation of ADNI and/or provided data but did not participate in analysis or writing of this report. A complete listing of ADNI investigators can be found at: http://adni.loni.usc.edu/wpcontent/uploads/how_to_apply/ADNI_Acknowledgement_List.pdf.

https://doi.org/10.1016/j.neuroimage.2021.118116.
Received 18 December 2020; Received in revised form 14 April 2021; Accepted 15 April 2021
Available online 1 May 2021.

scribed above. Moreover, the effects of stimulated echoes may go unnoticed leading to a stronger tendency to fit with a simple exponential decay, since the whole decay curve is not visible. Thus, the typical increased signal after the second refocusing pulse from stimulated echoes and subsequent oscillations are not seen. In addition, PD and T2-weighted sequences almost never prescribe 180° refocusing and will tend to use lower refocusing angles that are often varied along the echo train as well. Modelling approaches for these dual-echo sequences are less common, largely because the two data points do not enable fitting of more than two parameters, thus the transmit field effects must be known in advance. A more accurate two-point T2 fitting method employing Bloch simulations and RF pulse modelling in conjunction with prior knowledge of the refocusing flip angles was introduced by McPhee and Wilman, 2015 , which builds on the general idea of stimulated echo compensation to model the actual spin response (Ben-Eliezer et al., 2015; Lebel and Wilman, 2010). The two-echo Bloch modelling approach has been applied at a single site at 1.5T to examine T2 changes in the brain over 7 years in multiple sclerosis using retrospective clinical images (Uddin et al., 2017).

In this study, we wish to examine T2 mapping from PD and T2-weighted images across multiple sites and vendors. For example, in their inter-site study using the Alzheimer's Disease Neuroimaging Initiative (ADNI-1) database, Bauer et al., 2010 quantified T2 from exponential fitting of the PD and T2-weighted images and compared across sites and vendors at 1.5T. They reported highly variable T2 values and significant inter-site biases, concluding that there is a need for more elaborate methods for T2 quantification for multi-platform studies. The goal of our current work is to examine retrospective T2 quantification in the brain across multiple sites and vendors at 3T using dual-echo FSE images from the ADNI-1 database. We show that accounting for differences in pulse sequences and spatial variation in flip angle can enable comparison of T2 maps across sites and vendors.

2. Methods

2.1. MRI sequences and ADNI subjects

Retrospective brain MRI exams were downloaded from the ADNI-1 database (https://ida.loni.usc.edu/login.jsp?project=ADNI). Inclusion criteria were healthy subjects with available 3T scans from one of two vendors: Siemens Medical Systems (vendor 1) or General Electric Healthcare (vendor 2). A total of 24 subjects were found from 13 different sites in North America from the two MRI vendors. Fourteen healthy subjects (nine female, five male, mean age 73 years, range 59 – 80 years) were scanned with MRI systems from vendor 1, and the remaining ten (six female, four male, mean age 75 years, range 70 – 86 years) from vendor 2. All exams used a 2D dual FSE/TSE protocol with sequence parameters as follows: TE1 10.6 - 12.3 ms, TE2 95.2 - 99.0 ms, TR 3000 ms, 48 slices, voxel size $3.0 \times 0.94 \times 0.94$ mm^3, matrix size 256×228–256, 3 concatenations, and acquisition time 5 min. Both vendors used centric phase encode ordering for both the PD and T2-weighted images and parallel imaging was not used. Although most parameters for the 2D PD-T2 FSE were similar, the echo train length (ETL) and echo spacing differed between vendors: 14 echoes and 12.3 ms for vendor 1, 16 echoes and 10.6–10.8 ms for vendor 2. Importantly, the refocusing flip angle trains were very different. Vendor 1 used a refocusing flip angle train of mainly 150° while vendor 2 used different refocusing flip angle trains depending on the software release that varied between sites, including a constant 125° refocusing angle train, and a mainly 160° train. A pulse sequence diagram of an example FSE sequence is shown in Fig. 1.

To account for receive coil effects, ADNI-1 included two rapid 3D calibration scans, one of which used the transmit body coil for both excitation and signal reception. This calibration scan enabled estimation of the flip angle variation across the brain, a necessary input for the Bloch simulation based T2 fitting model when given only the two PD and T2-weighted decay data points (McPhee and Wilman, 2015). The 3D calibration scan was a single gradient echo sequence and the parameter specifications for both vendors were flip angle 2°, TE 1.1 – 1.3 ms, TR 2.9 – 3.4 ms, and ~40 s acquisition time. Voxel size was $2.5 \times 2.3 \times 2.3$ mm^3 for vendor 1 and $2.5 \times 1.2 \times 1.2$ mm^3 for vendor 2.

ADNI-1 also included data from Philips Healthcare systems, but this data did not include calibration scans since the FSE images were internally corrected for coil effects (Jack et al., 2008), so our method could not be applied.

2.2. Estimating $B1^+$ map from calibration images

We estimated $B1^+$ maps from the low flip angle calibration scan. The signal intensity, S of the calibration scan with respect to the receive RF field ($B1^-$) and transmit RF field ($B1^+$) for a rectangular RF pulse of duration t is given as:

$$S \propto B1^- \sin\left(\gamma B1^+ t\right) \tag{1}$$

Noting the small flip angle of 2°, Eq. (1) simplifies to:

$$S \propto \gamma t\, B1^- \times B1^+ \tag{2}$$

Further simplification can be made by making a rough assumption that for the body coil, $B1^- = B1^+$ in central brain regions at 3T (Vaidya et al., 2016). Hence, except for a normalization factor, the $B1^+$ field variation across the brain can be estimated simply by:

$$S \propto \left(B1^+\right)^2 \tag{3}$$

This approximation ignores T1 weighting given the small flip angle of 2°; however, the long T1 of cerebrospinal fluid (CSF) requires a correction for both increased T1-weighting and increased PD over grey and white matter.

To validate the $B1^+$ map estimation method from the calibration scan and determine its normalization factor, prospective acquisitions using the ADNI-1 3D calibration protocol were collected on a 3T Prisma (Siemens Medical Systems) for five additional healthy subjects (3 male, 2 female, mean 26 years, 21 – 31 years). These validation subjects also received a $B1^+$ map acquisition using the Bloch-Siegert method (Sacolick et al., 2010) to serve as the gold standard $B1^+$. All subjects provided written, informed consent and the local institutional ethics board approved this investigation. Scan parameters for the Bloch-Siegert $B1^+$ mapping were as follows: TE 2.2 ms, TR 19.7 s, voxel size $1.6 \times 1.6 \times 3.0$ mm^3, flip angle 5°, and acquisition time 40 s.

Normalized $B1^+$ ($nB1^+$) maps were created such that the nominal flip angle prescribed in the sequence corresponded to a value of 1.0. Estimated $nB1^+$ maps of the validation subjects were globally scaled to match with their respective Bloch-Siegert $nB1^+$ maps (or measured $nB1^+$ maps). The assumption that this method provides a sufficiently accurate $B1^+$ map estimate was verified by comparing the estimated $nB1^+$ map to the measured $nB1^+$ map using difference images and profile plots. Estimated $nB1^+$ maps for ADNI-1 subjects used the same global scaling.

2.3. T2 fitting model

T2 maps were generated from fitting of the dual-echo FSE data by modelling the actual RF pulses and slice select gradients used in each pulse sequence for each vendor. Bloch fitting utilized Indirect and Stimulated Echo Compensation (ISEC), as previously described (McPhee and Wilman, 2015). A flowchart for the T2 fitting model is illustrated in Fig. 2. The method models slice-selective RF pulses using the Shinnar-Le Roux (SLR) algorithm (Pauly et al., 1991). Ignoring relaxation effects during the pulses, the RF pulses were broken into 1024 hard pulse segments, equally spaced over the duration of the RF pulse. The SLR parameters were used to calculate the magnetization following each pulse segment. For slice selection modelling, magnetization response to RF pulses, gradients and relaxation were calculated at 1501 points equally spaced over thrice the excitation width. Relaxation decay between RF pulses were calculated by employing solutions to the Bloch

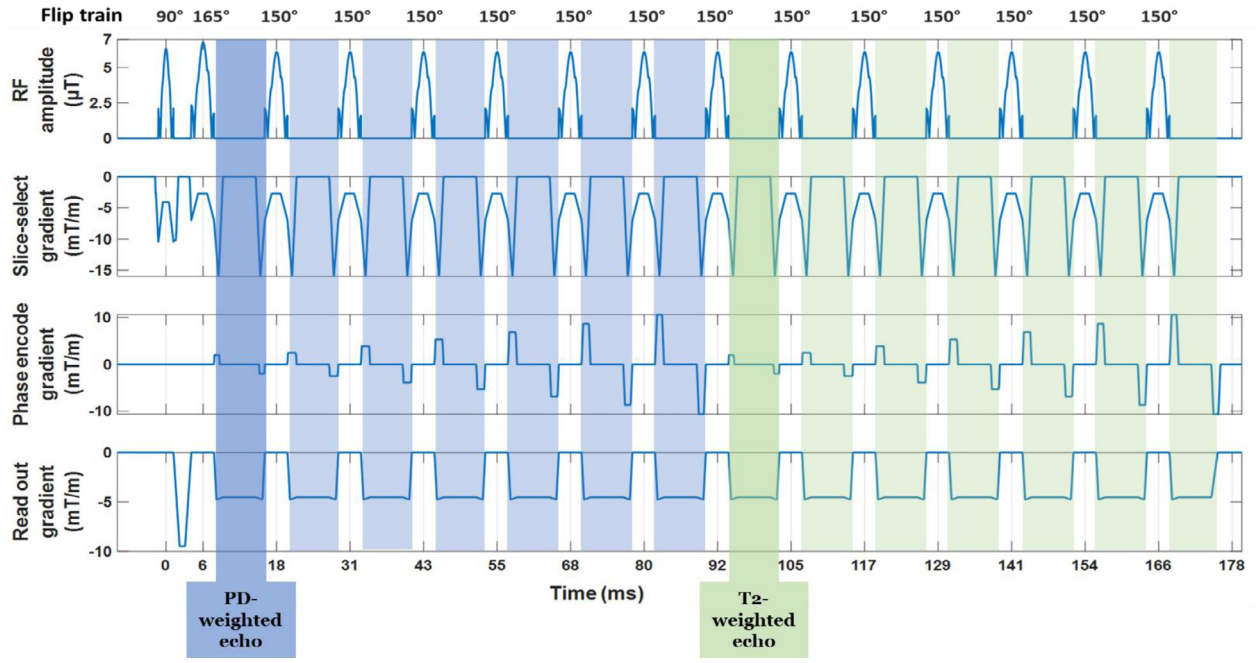

Fig. 1. Example dual-echo FSE pulse sequence using TE1 12.3 ms, TE2 99 ms and echo spacing 12.3 ms. The first seven echoes (blue) form the PD-weighted image and the next 7 echoes (green) the T2-weighted image. Centric phase encode order was used for both images with the effective TEs shown. Sequence variants between sites/vendors all use centric phase encoding. The most significant differences between vendors/sites was the refocusing pulses and flip angles. In this example from vendor 1, the flip angle train is 90°- 165°- 150°- 150°-.... The excitation and refocusing RF pulses were 2.56 ms and 3.85 ms in duration with the flat central portion of the RF pulse corresponding to a gradient strength of 0.4 G/cm for excitation and 0.27 G/cm for the refocusing. (For interpretation of the references to color in this figure legend, the reader is referred to the web version of this article.)

equations for transverse magnetization T2 decay and longitudinal magnetization T1 changes. Echo amplitudes were then calculated by summing the 1501 points together at each echo time. Similar to past work by Ben-Eliezer et al., 2015; the simulation does not model frequency or phase encode gradients since with adequate spoiling, the stimulated and indirect echoes arise only from the RF pulse and slice select gradient interactions. Note the phase encode is rewound after each acquisition and that the frequency encoding gradient remains constant for each readout (Fig. 1).

The simulation was repeated for a range of T2 and $B1^+$ values to create a dictionary of T2 decay curves. For the dictionary, simulations used a range of T2 from 10 – 1000 ms, with resolution at 0.2 ms resolution up to 150 ms, 1.0 ms from 150 – 200 ms, 2.0 ms from 200 – 300 ms, 5 ms from 300 – 500 ms, and 10 ms from 500 – 1000 ms. The high T2 digital resolution of 0.2 ms in the tissue range was used to ensure no digitization errors are compounded into the measurements. The longitudinal relaxation (T1) time was kept constant at 1 second, since T1 variations have very minor effects. The uniform T1 assumption for the Bloch based fitting model is evaluated in detail in McPhee and Wilman, 2015. The $nB1^+$ maps were provided as flip angle maps to the fitting algorithm. The nominal flip angles of each sequence were used along with an $nB1^+$ ranging from 0.40 – 1.40 at 0.005 resolution to account for the varying flip angle distribution across the brain due to RF interference. The computation time for the lookup dictionary generation depends on the number of simulated values of T2 and $B1^+$ and for the fitting part, it mainly depends upon the number of voxels to be fitted. Running on an Intel® Core™ i7–8750H CPU @2.20 GHz, for 891 T2 values, 201 $B1^+$ values and ETL=14, the lookup dictionary was generated in 23 min and the reconstruction time for an average sized brain was 1.2 min per slice, with 48 slices requiring ~ 1 hour. FSE data were fitted for T2 and amplitude via minimization of the sum squared difference. All simulations and fitting methods were performed using in-house MATLAB (R2018b, 64 bit) code. Standard two-point exponential fitting was also performed for comparison.

2.4. T2 analysis

The T2 maps were compared using whole-brain T2 histograms and manually drawn regions-of-interest (ROIs) from bilateral grey and white matter structures (Caudate, Putamen, Globus Pallidus, Thalamus, Genu, and Splenium). Mean ROI T2 values were reported, with multi-slice bilateral ROIs combined. The estimated $B1^+$ maps and measured $B1^+$ maps were co-registered and resliced to the dual-echo images' native space using the within-subject rigid body registration tool in Statistical Parameter Mapping (SPM-12). All brain images were skull-extracted using the Brain Extraction Tool (BET) in FMRIB Software Library (FSL v6.0).

Statistical analyses were conducted in R (version 4.0.2, 64 bit). Wilcoxon signed-rank test was used to compare the two fitting models. The validation T2 maps generated from measured and estimated $nB1^+$ maps were also compared with the same test. The Kolmogorov-Smirnov test was used to examine the whole-brain T2 histograms of the two vendors for peak T2 and T2-width (FWHM). A p-value of <0.05 was considered statistically significant.

3. Results

3.1. Validation of T2 fitting using $B1^+$ map estimation

An anecdotal example of $nB1^+$ maps obtained from the measured and estimated methods is shown in Fig. 3. The two $nB1^+$ maps show reasonable agreement in central regions with larger deviations near the edges of the brain. Example T2 maps generated with the two $nB1^+$ maps are shown in Fig. 4 for the same volunteer as in Fig. 3. Similar to the $nB1^+$ maps, there is a good accordance between the T2 maps in central portions; however, differences increase towards the edges of the brain.

Whole brain T2 histograms from all five validation subjects using the two $nB1^+$ maps are shown in Fig. 5. No significant differences were found between the average peak T2 ($p = 0.34$) nor the FWHM ($p = 0.37$).

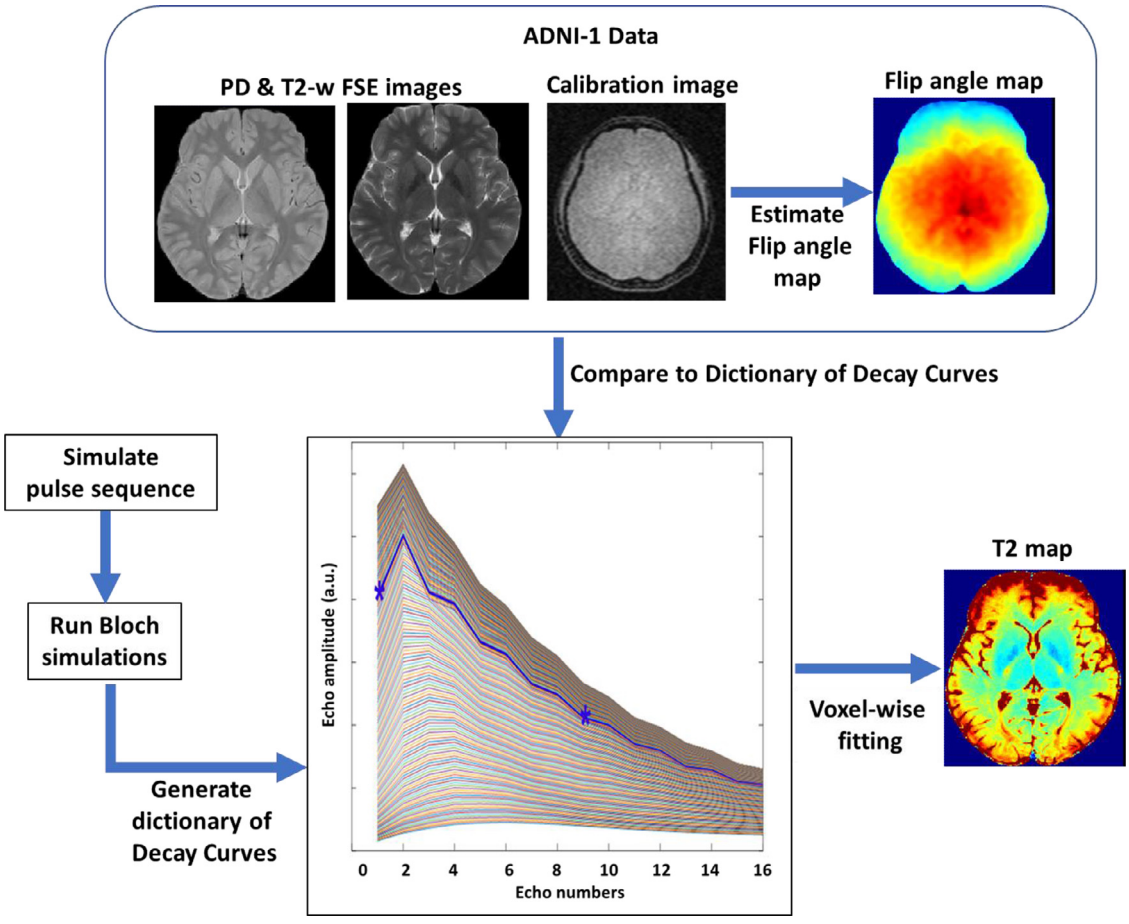

Fig. 2. Flow chart for the T2 fitting process. The flip angle map is estimated from the ADNI-1 calibration scan. Bloch based simulation of the FSE sequence is used to create a dictionary of T2 decay curves. The flip angle map is used to take a subset of data from the dictionary, and two-point T2 fitting is performed using the FSE images. The fitting algorithm finds the minimum of the sum squared residuals and T2 map is generated on a voxel by voxel basis. (For interpretation of the references to color in this figure legend, the reader is referred to the web version of this article.)

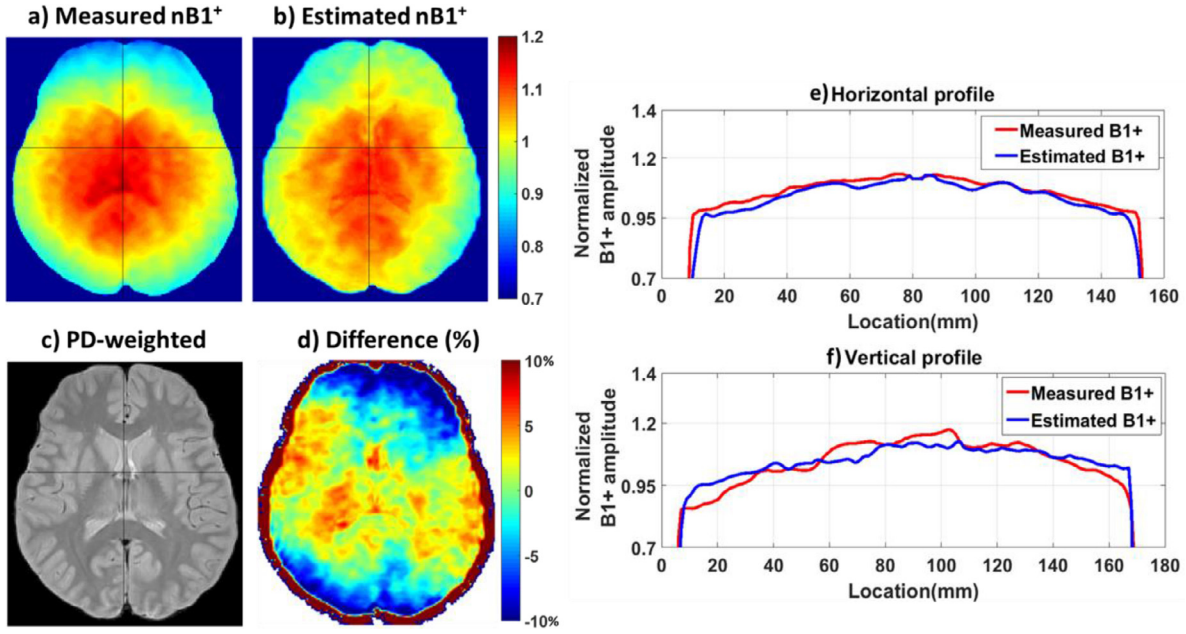

Fig. 3. Comparison of measured $nB1^+$ map (a) and estimated $nB1^+$ map (b) of a 26 yr old healthy female volunteer. The corresponding PD-weighted axial slice (c) and percentage difference image (d), (calculated as 100% × (a-b)/a) is shown. Normalized $B1^+$ map profiles obtained along the left-right and anterior-posterior directions are shown in (e) and (f) respectively. (For interpretation of the references to color in this figure legend, the reader is referred to the web version of this article.)

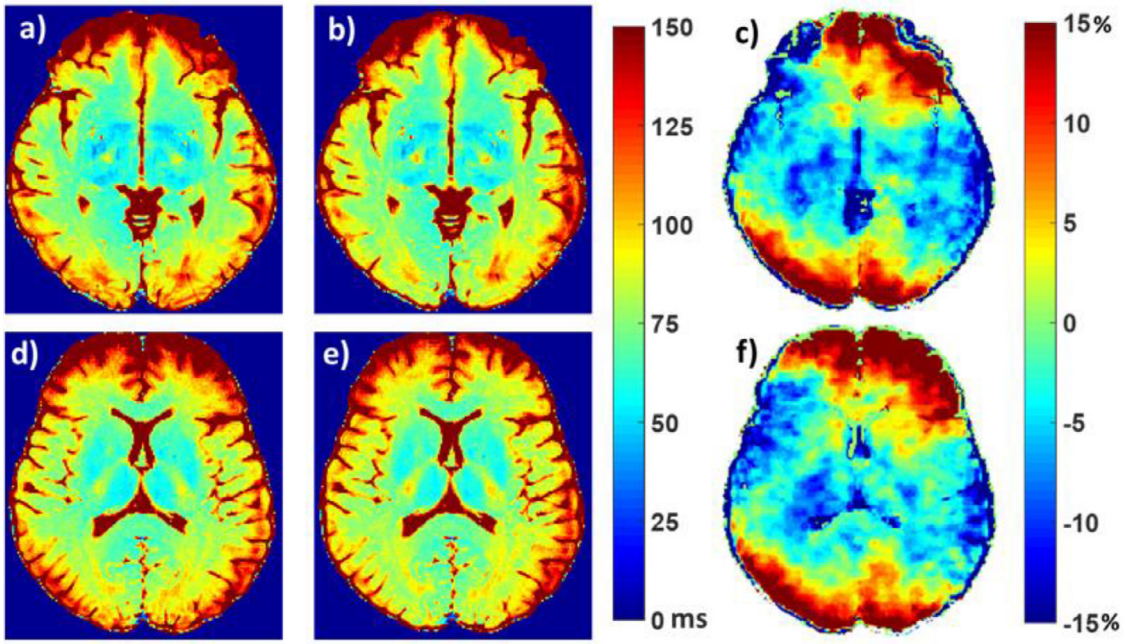

Fig. 4. T2 maps (ms) computed with the Bloch fit method for two different slices of a healthy 26 yr old female volunteer. T2 maps created with the measured nB1$^+$ map (a,d) and the estimated nB1$^+$ map (b, e) along with the percentage difference images (c, f) are shown (calculated as 100% × [(measured T2 - estimated T2)/measured T2)]. (For interpretation of the references to color in this figure legend, the reader is referred to the web version of this article.)

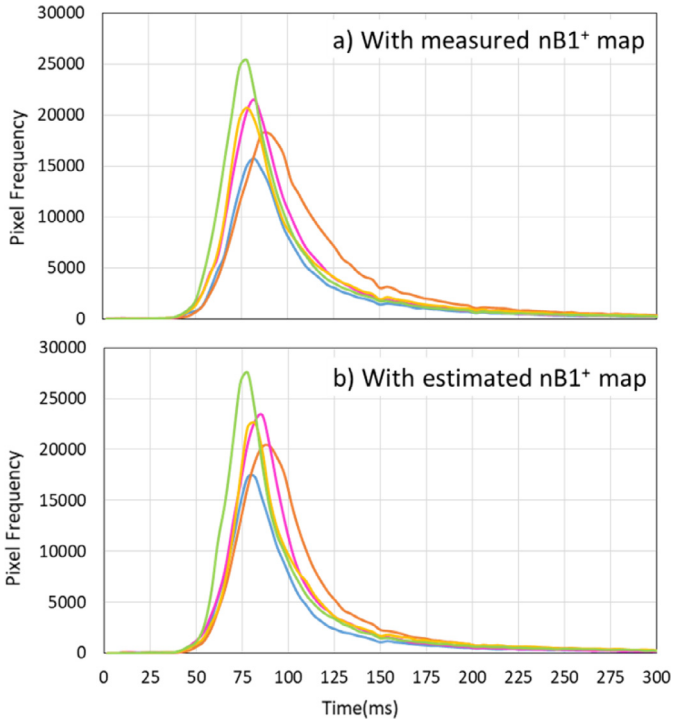

Fig. 5. Whole-brain histograms of T2 maps from five validation subjects obtained with measured (a) and estimated (b) nB1$^+$ maps. (For interpretation of the references to color in this figure legend, the reader is referred to the web version of this article.)

Mean T2 ROIs and the corresponding nB1$^+$ values from all the validation subjects are shown in Table 1. For these central ROIs, no significant differences are found in T2 or nB1$^+$ values (p>0.05). Mean T2 for CSF in lateral ventricles from all the validation subjects were found to be 401 ± 111 ms with measured nB1$^+$ maps and 450 ± 130 ms with estimated nB1$^+$ maps. These values underestimate the true CSF T2 of 2 s (Spijkerman et al., 2018) due to only sampling the decay curve up to 100 ms. CSF is not considered further, and only tissue T2 measures are reported for the ADNI-1 study, since the experiment is not designed to measure long T2 values in fluids.

3.2. T2 maps of ADNI-1 subjects

Example T2 maps of two different ADNI-1 subjects and their corresponding PD, T2-weighted images, and estimated nB1$^+$ maps are depicted in Fig. 6, where the exponential fit yields very different T2 maps (d,i), while the Bloch-fit results in similar T2 maps (e,j) between vendors/subjects. Vendor 1 used a refocusing flip train of 165°–150°–150°… .with an ETL of 14 and vendor 2 used a constant 125° flip train with ETL 16. The T2 maps displayed used PD/T2-weighted images with TE = 12.3, 99 ms for vendor 1, and TE = 10.6, 95.4 ms for vendor 2. Grayscale T2 maps for these subjects and a validation case are provided as supplementary materials.

Whole-brain T2 histograms from all ADNI-1 subjects from exponential and Bloch based fits are depicted in Fig. 7 for both vendors. Histograms are clipped at 300 ms. Peak T2 from the exponential fit were higher than the corresponding peak T2 from the Bloch fit in vendor 1 (p = 0.001) and vendor 2 (p = 0.005). Although the subjects are different between the vendors, we still expect similar (not same) T2's between vendors as they are all healthy subjects. T2 histograms from exponential fit showed significant differences in peak T2 values between the two vendors as well (p = 0.0002). On the contrary, peak T2 values between T2 histograms from Bloch fit were similar in values between the vendors (p = 0.12). For each T2 histogram, the width was measured at half maximum. Exponential fit of data from vendor 2 resulted in the broadest histograms (mean histogram width of 42 ms) and highest variance between the peak T2 values (standard deviation = 11.5 ms). Overall analysis showed a significant width difference between the T2 fitting models for vendor 2 (p = 0.006). With Bloch fit, there was no significant difference between the histogram widths of both vendors (p = 0.993).

Vendor-wise mean T2 from central brain ROIs of all ADNI-1 subjects are reported in Table 2. The Bloch fit T2's are much shorter than the

Table 1
Mean T2 (ms) and nB1$^+$ from all five volunteers.[a,b].

	Caudate	Putamen	Globus Pallidus	Thalamus	Genu	Splenium
measured nB1$^+$	1.06 ± 0.02	1.09 ± 0.02	1.12 ± 0.02	1.14 ± 0.03	1.00 ± 0.02	1.11 ± 0.02
mean T2 (ms)	72.1 ± 3.9	63.8 ± 3.2	49.8 ± 3.0	60.0 ± 2.0	72.3 ± 3.6	67.9 ± 4.3
estimated nB1+	1.08 ± 0.01	1.09 ± 0.02	1.11 ± 0.02	1.12 ± 0.02	1.01 ± 0.02	1.08 ± 0.01
mean T2 (ms)	70.3 ± 3.0	63.3 ± 2.4	50.4 ± 2.6	62.0 ± 1.0	70.0 ± 2.6	69.7 ± 4.4

[a] T2 maps were generated using the Bloch-based fit method. Data is reported as mean ± standard deviation.
[b] n=5 volunteers, aged 26.0 ± 3.6 years.

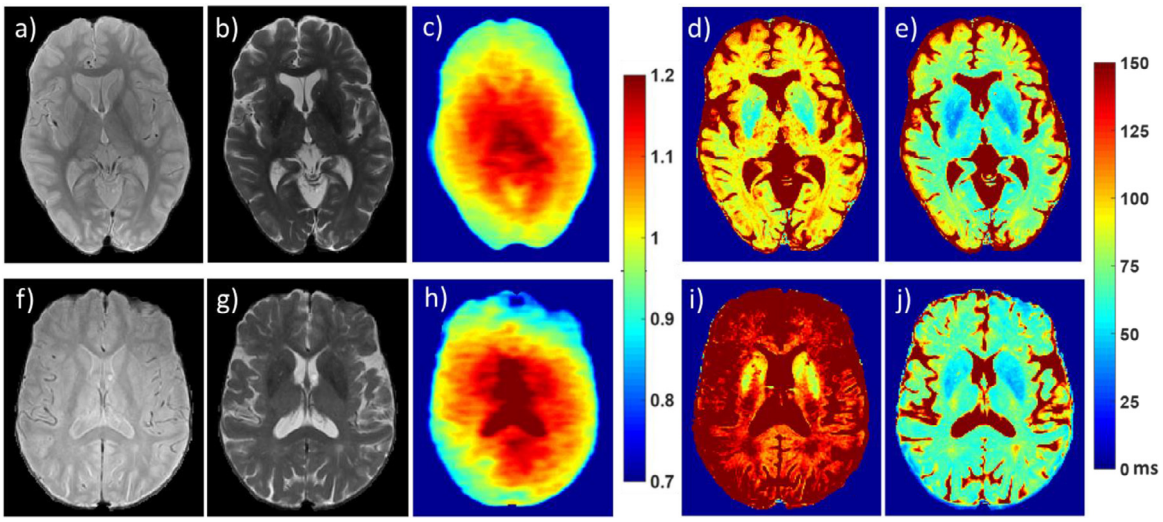

Fig. 6. Example images and resultant maps from two ADNI-1 subjects. Top Row: 77 yr healthy female from vendor 1 using a refocusing flip train of 165°–150°–150°-…. Bottom Row: 78 yr healthy female from vendor 2 using a refocusing flip train of constant 125° The input PD-weighted (a, f) and T2-weighted (b, g) images are shown along with estimated nB1$^+$ maps (c, h). T2 maps (ms) computed using exponential method (d, i) and Bloch based fit method (e, j) show the disparity in T2s between subject/vendor with the exponential approach but similarity with the Bloch method.

Table 2
Vendor-wise mean T2 (ms) and Coefficient of Variation (%) from ADNI-1 subjects. [a,b].

	Vendor 1		Vendor 2	
Region	**Exponential fit**	**Bloch fit**	**Exponential fit**	**Bloch fit**
Caudate	84.5 ± 5.8	56.3 ± 2.6	100.2 ± 9.2	60.9 ± 4.2
	6.9%	4.6%	9.2%	6.9%
Putamen	75.5 ± 4.5	52.2 ± 3.2	90.6 ± 12.1	55.6 ± 4.3
	6.0%	6.1%	13.4%	7.7%
Globus	67.0 ± 3.0	44.8 ± 2.4	72.7 ± 9.1	45.6 ± 4.6
Pallidus	4.5%	5.4%	12.5%	10.1%
Thalamus	92.2 ± 5.6	58.1 ± 2.8	96.1 ± 8.4	59.3 ± 3.1
	6.1%	4.8%	8.7%	5.2%
Genu	88.6 ± 5.1	65.4 ± 3.0	103.9 ± 10.7	61.9 ± 3.2
	5.8%	4.6%	10.3%	5.2%
Splenium	98.4 ± 4.9	66.1 ± 3.4	101.8 ± 10.1	62.0 ± 3.2
	5.0%	5.1%	9.9%	5.2%

[a] Vendor 1: n = 14, aged 73.0 ± 5.5 years, and Vendor 2: n = 10, aged 75.0 ± 4.2 years.
[b] T2 value is reported as mean ± standard deviation. Second row of each region shows the Coefficient of variation.

exponential fit (p = 0.03) and the standard deviations are reduced. Considering all ROIs, there were no significant differences between vendors in T2 values with Bloch fit (p = 0.93) nor with exponential fit (p = 0.47). With the Bloch fit, the mean absolute T2 difference between vendors for all ROIs was only 2.9 ± 0.9 ms, while exponential fit was 11.1 ± 5.2 ms. Note that the two groups used different subjects so exact agreement is not expected.

4. Discussion

T2 maps computed with the Bloch simulation based fitting of the PD and T2-weighted images resulted in similar T2 values across vendors and sites. In contrast, T2 maps computed with an exponential fit resulted in histograms with remarkably increased peak T2 (p = 0.001 for vendor 1 and p = 0.005 for vendor 2) and broader FWHM for vendor 2 (p = 0.006). These biases in T2 measurements were minimized by accounting for indirect and stimulated echo contamination, via modelling of the pulse sequences, using known refocusing flip angles and estimated B1$^+$ maps to account for RF field inhomogeneity. The low flip angle calibration scan of the ADNI-1 data set enabled an estimation of B1$^+$ maps, which was validated in comparison to measured B1$^+$ maps in a cohort of healthy volunteers. Note that for the two-point fitting approach, the B1$^+$ map cannot be determined as part of the fitting process, since there are already two unknowns of initial signal and T2 value. For the ADNI-1

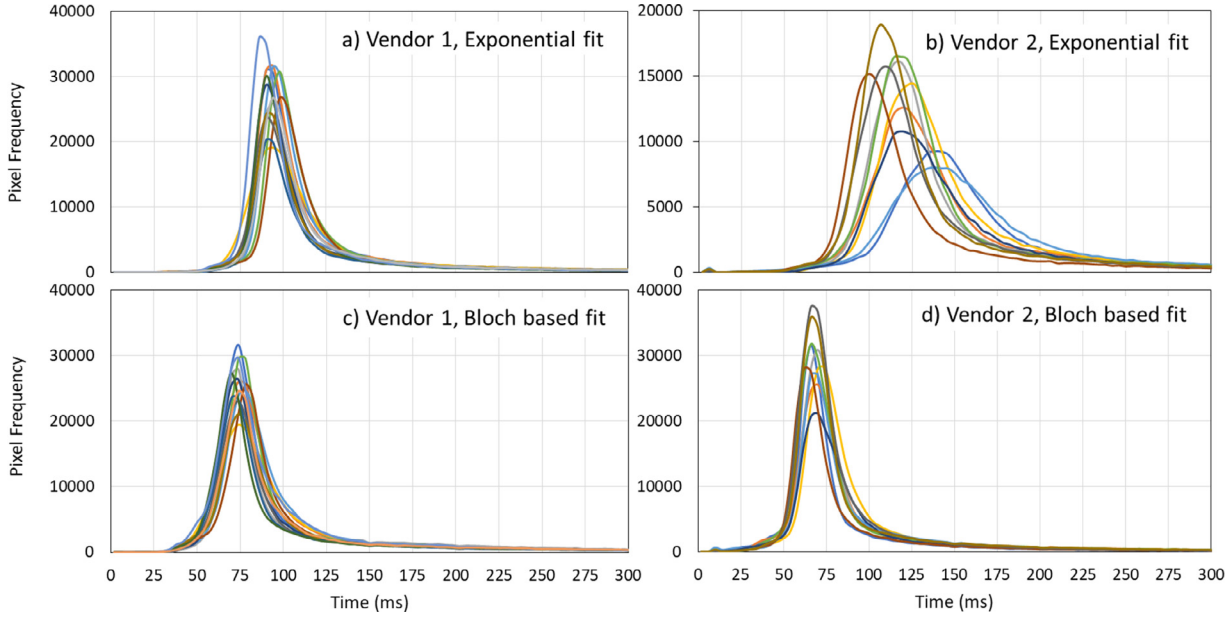

Fig. 7. Whole-brain histograms of T2 maps from 24 ADNI-1 subjects using two vendors- 14 subjects from vendor 1 (a, c) and 10 subjects from vendor 2 (b, d). Histograms from exponential fit (a, b) and Bloch based fit (c, d). Note different scale for y-axis in (b).

data with Bloch based fit, there were no significant differences in peak T2 ($p = 0.12$) and FWHM ($p = 0.993$) between the T2 maps from the two vendors.

The specific goal of our work was to demonstrate that if the differences in pulse sequences between vendors and sites are accounted for, the bias between sites/vendors can be minimized. Previous work has recognized the need for pulse sequence modelling to account for indirect and stimulated echoes, and remove T2 overestimation that is typically observed with fitting of MESE or FSE data with an exponential decay function (Lebel and Wilman, 2010; Ben-Eliezer et al., 2015; McPhee and Wilman, 2015; Nöth et al., 2017). As shown here, these T2 errors are compounded for inter-site and inter-vendor studies when RF pulse parameters vary between sites. ADNI-1 standardized most sequence timing parameters between sites and vendors with only slight variations in effective echo times, echo spacing and ETL; however, each vendor used its own RF pulse shapes and refocusing flip angle trains, which we accounted for in our modelling. For example, vendor 1 used the same refocusing flip angle train between all of its sites, while vendor 2 used different refocusing angles that also varied between software versions. These sequence variations make standard exponential fitting unacceptable for multi-vendor T2 studies, as was found by Bauer et al., 2010 with 1.5T data.

More generally, to accurately simulate any 2D FSE/TSE sequence variation, the refocusing flip angle train must be known. This includes all the sequence timing parameters, the nominal refocusing angles which may vary throughout the train, the RF pulse shapes, and the relative strength of the slice select gradients for the excitation and refocusing pulses. In cases where the full pulse sequence parameters are not known, Nöth et al., 2017 demonstrated that by careful measurements with a phantom of known T2, a correction scheme could be devised; however, this approach requires prospective experiments on each scanner and may have difficulty with variable angle trains.

Clearly, accurate T2 becomes increasingly difficult as one reduces the number of data points. In the limit of two data points available here, precise modelling of the pulse sequence becomes essential to minimize additional errors. Nevertheless, the accuracy of the T2 fit is impacted by the choice of the two effective echo times available for fitting, the refocusing flip angle train and the available SNR (McPhee and Wilman, 2015). For example, the longest echo point in the ADNI-1 data was ~100 ms, which is insufficient to accurately estimate long fluid T2s like CSF (Spijkerman et al., 2018). As a general guideline, considering a conservative SNR of 30 in the PD image, T2s up to 300 ms can be measured within ±5% accuracy, if $B1^+$ is also measured to within ±5% accuracy. Higher accuracy in $B1^+$ would extend the T2 range somewhat; however, the ultimate T2 maximum limit would also depend on the exact flip angle scheme. In addition, the two-point fitting method cannot account for multi-component T2 relaxation, which is most commonly noted in white matter (Whittall et al., 1997). Multi-compartment T2 relaxometry methods (Prasloski et al., 2012) rely on sampling the T2 decay curve at multiple echo times (typically 32) and involve a large number of unknown parameters to fit. With only two-echo points, our method provides a single T2 component approximation which is all that is possible from clinical data sets using PD and T2-weighting.

Differences in phase encoding orders are also important when using FSE images, especially if the PD and T2-weighted images use different ordering that would cause different point spread function (PSF) effects (Anderson et al., al.,2013). For ADNI-1 data, both vendors employed centric phase encode ordering for the PD and T2-weighted images. Furthermore, relatively short echo trains were used with 7 or 8 echoes per image. This further limited PSF effects and also made the modelling of only the effective TE's sufficient to account for the image contrast. For example with a 7 echo train, the most central 14% of the phase encodes were all acquired at the exact TE, which would dominate the image contrast.

In the literature there is a wide range of T2 values at 3T depending on the methods used. Using structures putamen, thalamus and globus pallidus, the T2 values obtained in this study at 3T are similar to those found with past methods that either accounted for stimulated and indirect echoes (Nöth et al., 2017), or chose to eliminate the effects through adiabatic refocusing (Mitsumori et al., 2012). Nevertheless there are a wide range of reported T2 values in the literature for brain owing to differing approaches being applied, with exponential fitting curves yielding large overestimates (Kumar et al., 2012; Sedlacik et al., 2014).

One limitation was a lack of true $B1^+$ maps in the ADNI-1 retrospective data, requiring estimation of $B1^+$ maps from the ADNI-1 calibration scans. This method was validated in a small prospective study. Although the $B1^+$ estimation error increases towards the brain edges, the validation results showed that the estimated $B1^+$ maps are similar in central

parts of the brain and whole brain histograms were not impacted. Nevertheless we focused our ROI measures on central brain regions where the calibration assumption of body coil transmit $B1^+$ and body coil receive $B1^-$ equivalency is more accurate. While the ADNI-1 calibration scan was sufficient to estimate $B1^+$ map, prospective studies could use a rapid $B1^+$ mapping technique for greater precision. The slow variation of $B1^+$ in the head allows for low resolution $B1^+$ maps, which can now be acquired rapidly (Lesch et al., al.,2019). An additional limitation was the lack of a gold standard T2 comparison in the ADNI data set. Nevertheless, using a PD and T2-weighted sequence with actual $B1^+$ maps has previously shown that human brain tissue T2 values obtained with this fitting method are similar when compared against fitting of a 32 echo MESE sequence (McPhee and Wilman, 2015).

Conclusion

We examined retrospective T2 mapping across multiple sites and two vendors using standard PD and T2-weighted images of brain. With standard exponential fitting, large T2 biases were observed between vendors. By using Bloch-based modelling of the pulse sequence and estimating the $B1^+$ field, biases in T2 values between sites and vendors were minimized. The use of standard PD and T2-weighted images enables quantitative T2 measurement at the same spatial resolution as standard weighted images with no additional imaging time. Bloch modelling of the actual refocusing angles enables T2 quantification from PD and T2-weighted images across multiple sites and vendors.

Data and code availability statement

The code for T2 fitting is available for sharing from the corresponding author on reasonable request.

The images used for the multi-site and multi-vendor study are available from the Alzheimer's Disease Neuroimaging Initiative (ADNI) database (https://ida.loni.usc.edu/login.jsp?project=ADNI).

Credit author statement

Gitanjali Chhetri: Methodology, Software, Investigation, Writing - Original Draft, Writing - Review & Editing

Kelly C. McPhee: Methodology, Software, Investigation, Writing - Review & Editing

Alan H. Wilman: Conceptualization, Funding acquisition, Supervision, Writing - Review & Editing

Declarations of Competing Interest

None.

Acknowledgement

Data collection and sharing for this project was funded by ADNI (National Institutes of Health Grant U01 AG024904) and DOD ADNI (Department of defense award number W81XWH-12–2–0012). ADNI is funded by the National Institute on Aging, the National Institute of Biomedical Imaging and Bioengineering, and through generous contributions from the following: AbbVie, Alzheimer's Association; Alzheimer's Drug Discovery Foundation; Araclon Biotech; BioClinica, Inc.; Biogen; Bristol-Myers Squibb Company; CereSpir, Inc.; Cogstate; Eisai Inc.; Elan Pharmaceuticals, Inc.; Eli Lilly and Company; EuroImmun; F. Hoffmann-La Roche Ltd and its affiliated company Genentech, Inc.; Fujirebio; GE Healthcare; IXICO Ltd.;Janssen Alzheimer Immunotherapy Research & Development, LLC.; Johnson & Johnson Pharmaceutical Research & Development LLC.; Lumosity; Lundbeck; Merck & Co., Inc.;Meso Scale Diagnostics, LLC.; NeuroRx Research; Neurotrack Technologies; Novartis Pharmaceuticals Corporation; Pfizer Inc.; Piramal Imaging; Servier; Takeda Pharmaceutical Company; and Transition Therapeutics. The Canadian Institutes of Health Research is providing funds to support ADNI clinical sites in Canada. Private sector contributions are facilitated by the Foundation for the National Institutes of Health (www.fnih.org). The grantee organization is the Northern California Institute for Research and Education, and the study is coordinated by the Alzheimer's Therapeutic Research Institute at the University of Southern California. ADNI data are disseminated by the Laboratory for Neuro Imaging at the University of Southern California.

We would like to thank Peter Šereš for assistance with data collection. Grant support was provided by the Canadian Institutes of Health Research.

Supplementary materials

Supplementary material associated with this article can be found, in the online version, at doi:10.1016/j.neuroimage.2021.118116.

References

Anderson, S.W., Sakai, O., Soto, J.A., Jara, H., 2013. Improved T2 mapping accuracy with dual-echo turbo spin echo: effect of phase encoding profile orders. Magn. Reson. Med 69 (1), 137–143. doi:10.1002/mrm.24213, https://doi.org/.

Bartzokis, G., Sultzer, D., Lu, P.H., Nuechterlein, K.H., Mintz, J., Cummings, J.L., 2004. Heterogeneous age-related breakdown of white matter structural integrity: implications for cortical "disconnection" in aging and Alzheimer's disease. Neurobiol. Aging 25, 843–851. doi:10.1016/j.neurobiolaging.2003.09.005, https://doi.org/.

Bauer, C.M., Jara, H., Killiany, R., 2010. Whole brain quantitative T2 MRI across multiple scanners with dual echo FSE: applications to AD, MCI, and normal aging. Neuroimage 52, 508–514. doi:10.1016/j.neuroimage.2010.04.255, https://doi.org/.

Ben-Eliezer, N., Sodickson, D.K., Block, K.T., 2015. Rapid and accurate T2 mapping from multi-spin-echo data using bloch-simulation-based reconstruction. Magn. Reson. Med. 73, 809–817. doi:10.1002/mrm.25156, https://doi.org/.

Cheng, H.M., Stikov, N., Ghugre, N.R., Wright, G.A., 2012. Practical medical applications of quantitative MR relaxometry. J Magn Reson Imag 36, 805–824. doi:10.1002/jmri.23718, https://doi.org/.

Deoni, S.C.L., 2010. Quantitative relaxometry of the brain. Top Magn Reson Imaging 21 (2), 101–113. doi:10.1097/RMR.0b013e31821e56d8, https://doi.org/.

Emmerich, J., Flassbeck, S., Schmidt, S., Bachert, P., Ladd, M.E., Straub, S., 2019. Rapid and accurate dictionary-based T2 mapping from multi-echo turbo spin echo data at 7 Tesla. J. Magnet. Reson. Imaging 49 (5), 1253–1262. doi:10.1002/jmri.26516, https://doi.org/.

Hasan, K.M., Walimuni, I.S., Kramer, L.A., Frye, R.E., 2010. Human brain atlas-based volumetry and relaxometry: application to healthy development and natural aging. Magn. Reson. Med. 64 (5), 1382–1389. doi:10.1002/mrm.22515, https://doi.org/.

Hennig, J., 1991. Echoes—how to generate, recognize, use or avoid them in MR-imaging sequences. Part II: echoes in imaging sequences. Concepts Magn. Reson. 3, 179–192. doi:10.1002/cmr.1820030402, https://doi.org/.

Hennig, J., Nauerth, A., Friedburg, H., 1986. RARE imaging: a fast imaging method for clinical MR. Magn. Reson. Med. 3, 823–833. doi:10.1002/mrm.1910030602, https://doi.org/.

Jack Jr, C.R., Bernstein, M.A., Fox, N.C., Thompson, P., Alexander, G., Harvey, D., Borowski, B., Britson, P.J.L., Whitwell, J., Ward, C., Dale, A.M., 2008. The Alzheimer's disease neuroimaging initiative (ADNI): MRI methods. J. Magnet. Reson. Imaging 27 (4), 685–691. doi:10.1002/jmri.21049, https://doi.org/.

Knight, M.J., McCann, B., Tsivos, D., Couthard, E., Kauppinen, R.A., 2016. Quantitative T1 and T2 MRI signal characteristics in the human brain: different patterns of MR contrasts in normal ageing. Magn. Reson. Mater. Physics, Biol. Med. 29, 833–842. doi:10.1007/s10334-016-0573-0, https://doi.org/.

Kumar, R., Delshad, S., Woo, M.A., Macey, P.M., Harper, R.M., 2012. Age-related regional brain T2-relaxation changes in healthy adults. J. Magnet. Reson. Imaging 35 (2), 300–308. doi:10.1002/jmri.22831, https://doi.org/.

Lebel, R.M., Wilman, A.H., 2010. Transverse relaxometry with stimulated echo compensation. Magn. Reson. Med. 64, 1005–1014. doi:10.1002/mrm.22487, https://doi.org/.

Lesch, A., Schlöegl, M., Holler, M., Bredies, K., Stollberger, R., 2019. Ultrafast 3D Bloch-Siegert B1+ mapping using variational modeling. Magn Reson Med 81 (2), 881–892. doi:10.1002/mrm.27434, https://doi.org/.

MacKay, A., Laule, C., Vavasour, I., Bjarnason, T., Kolind, S., Mädler, B., 2006. Insights into brain microstructure from the T2 distribution. Magn. Reson. Imaging. doi:10.1016/j.mri.2005.12.037, https://doi.org/.

Majumdar, S., Orphanoudakis, S.C., Gmitro, A., O'Donnell, M., Gore, J.C., 1986. Errors in the measurements of T2 using multiple-echo MRI techniques. I. Effects of radiofrequency pulse imperfections. Magn. Reson. Med. 3, 397–417. doi:10.1002/mrm.1910030305, https://doi.org/.

McPhee, K.C., Wilman, A.H., 2015. T2 quantification from only proton density and T2-weighted MRI by modelling actual refocusing angles. Neuroimage 118, 642–650. doi:10.1016/j.neuroimage.2015.05.079, https://doi.org/.

Mitsumori, F., Watanabe, H., Takaya, N., Garwood, M., Auerbach, E.J., Michaeli, S., Mangia, S., 2012. Toward understanding transverse relaxation in human brain through its field dependence. Magn Reson Med 68 (3), 947–953. doi:10.1002/mrm.23301, https://doi.org/.

Nöth, U., Shrestha, M., Schüre, J.R., Deichmann, R., 2017. Quantitative in vivo T2 mapping using fast spin echo techniques-A linear correction procedure. Neuroimage 157, 476–485. doi:10.1016/j.neuroimage.2017.06.017, https://doi.org/.

Pauly, J., Nishimura, D., Macovski, A., Roux, P.Le, 1991. Parameter relations for the Shinnar-Le Roux selective excitation pulse design algorithm. IEEE Trans. Med. Imaging 10, 53–65. doi:10.1109/42.75611, https://doi.org/.

Prasloski, T., Mädler, B., Xiang, Q.S., MacKay, A., Jones, C., 2012. Applications of stimulated echo correction to multicomponent T2 analysis. Magn Reson Med 67 (6), 1803–1814. doi:10.1002/mrm.23157, https://doi.org/.

Petrovic, A., Scheurer, E., Stollberger, R., 2015. Closed-form solution for T2 mapping with nonideal refocusing of slice selective CPMG sequences. Magn Reson Med 73 (2), 818–827. doi:10.1002/mrm.25170, https://doi.org/.

Sacolick, L.I., Wiesinger, F., Hancu, I., Vogel, M.W., 2010. B1 mapping by Bloch-Siegert shift. Magn. Reson. Med. 63, 1315–1322. doi:10.1002/mrm.22357, https://doi.org/.

Schenck, J.F., Zimmerman, E.A., 2004. High-field magnetic resonance imaging of brain iron: birth of a biomarker? NMR Biomed doi:10.1002/nbm.922, https://doi.org/.

Sedlacik, J., Boelmans, K., Löbel, U., Holst, B., Siemonsen, S., Fiehler, J., 2014. Reversible, irreversible and effective transverse relaxation rates in normal aging brain at 3T. Neuroimage 84, 1032–1041. doi:10.1016/j.neuroimage.2013.08.051, https://doi.org/.

Spijkerman, J.M., Petersen, E.T., Hendrikse, J., Luijten, P., Zwanenburg, J.J.M., 2018. T2 mapping of cerebrospinal fluid: 3 T versus 7 T. MAGMA. 31 (3), 415–424. doi:10.1007/s10334-017-0659-3, https://doi.org/.

Uddin, M.N., McPhee, K.C., Blevins, G., Wilman, A.H., 2017. Recovery of accurate T2 from historical 1.5 tesla proton density and T2-weighted images: application to 7-year T2 changes in multiple sclerosis brain. Magn. Reson. Imaging 37, 21–26. doi:10.1016/j.mri.2016.11.007, https://doi.org/.

Vaidya, M.V., Collins, C.M., Sodickson, D.K., Brown, R., Wiggins, G.C., Lattanzi, R., 2016. Dependence of B1- and B1+ field patterns of surface coils on the electrical properties of the sample and the MR operating frequency. Concepts Magn. Reson. Part B Magn. Reson. Eng. 46, 25–40. doi:10.1002/cmr.b.21319, https://doi.org/.

Vymazal, J., Righini, A., Brooks, R.A., Canesi, M., Mariani, C., Leonardi, M., Pezzoli, G., 1999. T1 and T2 in the brain of healthy subjects, patients with Parkinson disease, and patients with multiple system atrophy: relation to iron content. Radiology 211, 489–495. doi:10.1148/radiology.211.2.r99ma53489, https://doi.org/.

Whittall, K.P., Mackay, A.L., Graeb, D.A., Nugent, R.A., Li, D.K., Paty, D.W., 1997. In vivo measurement of T2 distributions and water contents in normal human brain. Magn. Reson. Med. 37 (1), 34–43. doi:10.1002/mrm.1910370107, https://doi.org/.